II. MULTIMODAL PLATFORM FOR RAMAN AND NONLINEAR OPTICAL MICROSCOPY AND MICROSPECTROSCOPY FOR CONDENSED MATTER STUDIES

In 2016, the research activities of the Raman Spectroscopy Sector were focused mainly on accomplishing the following objectives:

– highly sensitive, contrast, and, most notably, noninvasive imaging of biological samples using Raman scattering microscopy and nonlinear optics methods (CARS, SHG);

– further increase in the concentration sensitivity limit of sample measurements by the SERS method at a level no worse than 10^{-10} M;

– acquisition of new data on photo- and upconversion luminescence in glass-ceramics based on nanosized ZnO crystals doped with rare-earth elements.

In addition, methodological studies aimed at further upgrading and modification of the CARS microscope were carried out during the period under review.

The Sector was also very active within the JINR Educational Programme in engaging students, postgraduates, and young scientists from the JINR Member States in its research for different periods of time.

1. Further modified "CARS" microscope

Figure 1-II-1 shows an optical diagram of the CARS microscope modified in 2016. To allow complementary imaging of the samples under investigation using not only nonlinear CARS microscopy but also the second harmonic generation (SHG), the corresponding narrow-band filters (532 nm Maxline) were added to the optical train, and sample excitation for generation of the second harmonic in it was performed with the Stokes frequency of a picosecond cw laser.

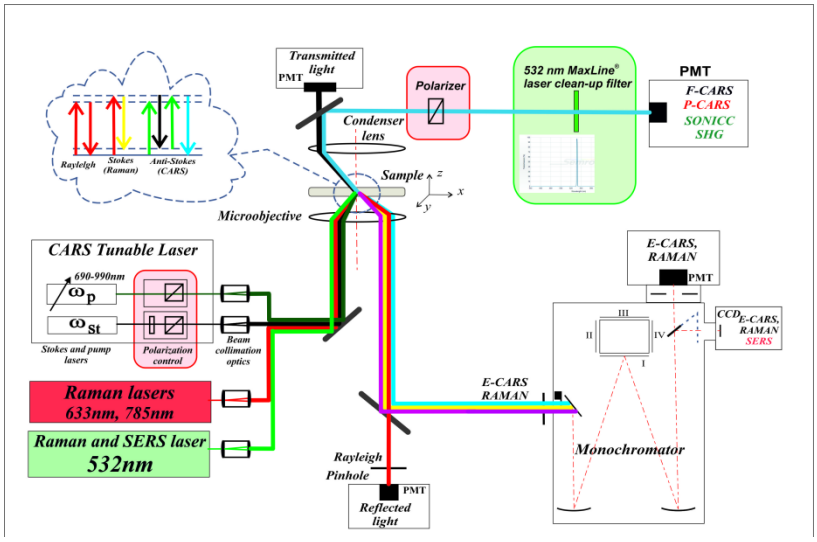

Fig. 1-II-1. Diagram of the modified "CARS" microscope: two new options are introduced.

In addition, an option was developed and installed, which allows the Raman scattering to be measured on samples excited at a wavelength of 785 nm, which is very important when working with samples with high autofluorescence background.

Using this optical platform, samples can be imaged by utilizing vibrational frequencies in the spectral range of (1000−3580) cm^{-1}, which covers all most important vibrational modes of bio-molecules. Five detection channels allow two forward- and three backward- propagated signals to be recorded. The polarization control is adjustable with a half-wave plate in the Stokes beam.

2. Scientific results

2.1. Highly Sensitive Coherent anti-Stokes Raman Scattering Imaging of Protein Crystals

In the reporting period, the work (started in 2015) on highly sensitive and high-speed visualization of protein crystals using the polarized coherent anti-Stokes Raman scattering (P-CARS) and the second harmonic generation (SHG) was completed.

It is well known that serial crystallography at last generation X-ray synchrotron sources and free electron lasers have enabled data collection with micrometer and even sub-micrometer size crystals resulting in amazing progress in structural biology. However, imaging of small crystals which although is highly demanded remains a challenge, especially in the case of membrane protein crystals.

CARS microscopy provides an advanced nondestructive and label-free technique with high sensitivity and high lateral spatial resolution capable of selective chemical imaging of major types of macromolecules: proteins, lipids, nucleic acids, etc.

Along with the P-CARS modality, in 2016 we developed a nonlinear imaging technique based on SONICC (Second Order Nonlinear Imaging of Chiral Crystals) technology for identifying chiral crystals, which relies on SHG (Second Harmonic Generation) and UV-TPEF (Ultraviolet Two Photon Excited Fluorescence) techniques. SONICC makes it easy to visualize microcrystals, including also optically-obscured crystals buried in meso matrix. Nevertheless, the technique fails when there are salt crystals in the probe and/or protein crystals with high symmetry classes. In the latter case the crystals will generate poorly detectable SHG signal scattering. In addition, at the moment there is no sufficiently cheap option of an SHG device for crystal imaging, therefore a search for new complementary approaches to crystals' studies and imaging might be very important.

The obtained main results are illustrated in **Fig. 1-II-2**.

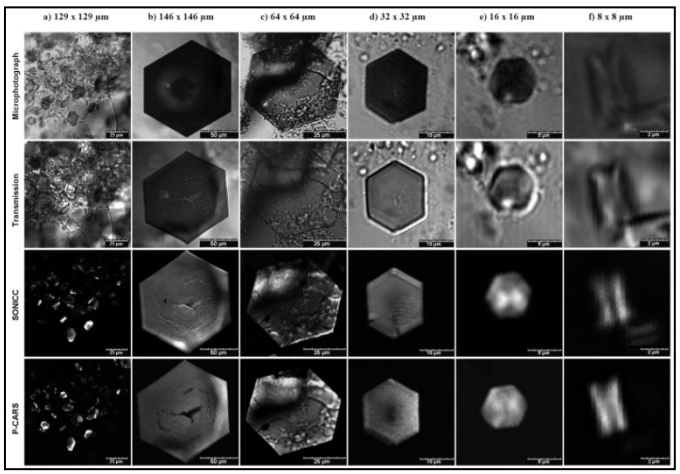

***Fig. 1-II-2**. Gallery of micrograph, transmission, SHG (SONICC) and P-CARS images of bR crystals acquired in various modes: (a) panoramic picture of a crystallization probe, (b, c) big crystals, (d) intermediate size crystals, (e and f) very small crystals.*

Also, we observed that in the case of some crystals (**Fig. 1-II-3**) the shape and/or size of the same crystals imaged by CARS and SHG are different. We suggest that it happens when some parts of the crystals are not well ordered. It is known that an SHG signal is strong only when the crystal is well ordered. It is of interest because a complementary use of both methods can provide information about the level of order in crystal packing and help to select crystals preliminarily for X-ray crystallography. It can be very useful because quite often the crystals may have a perfect shape but do not diffract at all.

Amazing sensitivity of the P-CARS imaging is further demonstrated by the detection and imaging of merohedrally twinned bR crystals (**Fig. 1-II-3**). Merohedral twinning is one of the most common crystal-growth defects. There is neither a fast approach to the detection of twinned crystals nor an efficient method to determine the twinning ratio. Twinned crystals cannot be optically distinguished. The only reliable method to detect crystal twinning is X-ray crystallography, which requires time-consuming X-ray data collection. In our work, we studied the potential of CARS for the detection of such crystals.

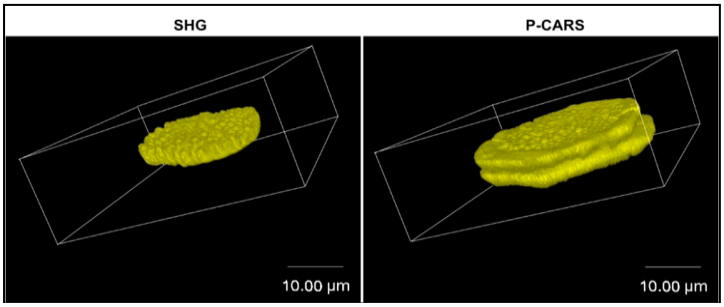

***Fig. 1-II-3**. 3D SHG and 3D P-CARS images of a twinned bR crystal. Box size: 48×48×24 µm. Images were obtained with 6 ps laser.*

Figure 1-II-3 demonstrates that the twinning of bR can be easily detected even in the case of small crystals with a micrometer size thickness, whereas an SHG signal with 6-ps excitation hardly discriminates the morphology of the twinned crystal if it partly consists of low-ordered segments. In contrast to X-ray crystallography, CARS makes the characterization of their morphology possible and demonstrates that the crystal consists of two nearly equal domains with a thickness of about 2.5 µm.

Thus, CARS, especially P-CARS, can be successfully applied for fast, high-resolution, high-contrast and very informative imaging of protein crystals. The CARS and SHG images are composed of 500 × 500 pixels taken by raster scanning the sample. Signal integration time was 3 µs/pixel.

The research was performed in close cooperation with Russian, French, and Belarusian scientists. All the experimental work on Raman imaging of the samples was done using the CARS microscope.

2.2. Detection of biomolecules by SERS spectroscopy

During the period under review considerable advances have been made in SERS research. In particular, the concentration sensitivity limit at a level of 10^{-10} M has been obtained for DNA molecules. It is 2–3 orders of magnitude better than in 2015.

The research was carried out with SERS-active substrates developed in Belarus on the basis of porous silicon and silver nanoparticles. Porous silicon was fabricated by electrochemical

anodic etching of a highly doped n-type silicon wafer. It has been found that silvered porous silicon is SERS active in relation to herring sperm DNA under the excitation at 473, 633 and 785 nm (**Fig. 1-II-4**). Laser powers were 1.45, 0.68, and 0.86 mW, respectively.

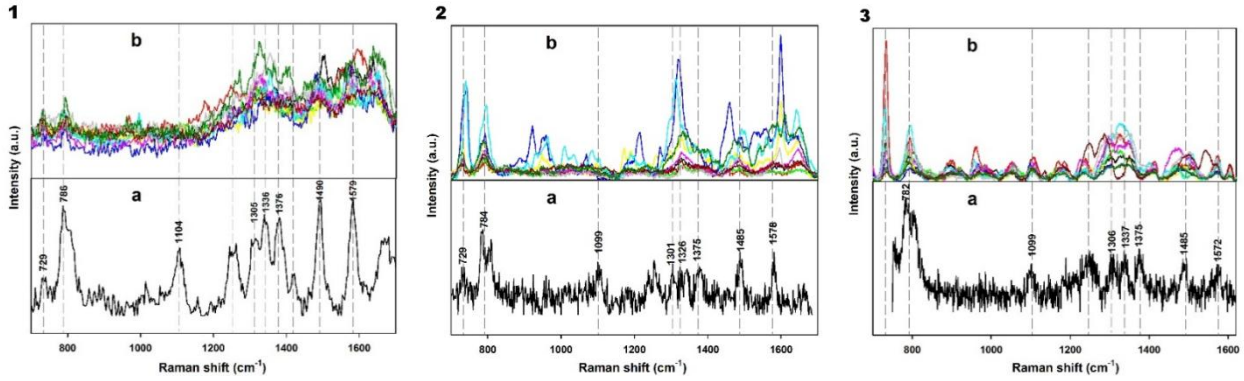

***Fig.1-II-4**. Raman (a) and SERS (b) spectra of 10–8-M herring sperm DNA collected at excitation wavelengths of 473 (1), 633 (2) and 785 (3) nm.*

The peaks observed in the Raman spectra around 730 cm^{-1} (adenine), 787 cm^{-1} (thymine, cytosine), 1104 cm^{-1} (ν(C-O), deoxyribose-phosphate), 1242 cm^{-1} (cytosine, adenine), 1381 cm^{-1} (thymine, guanine, гуанин, adenine), 1490 cm^{-1} (guanine, adenine) and 1581 cm^{-1} (guanine, adenine) are the characteristic Raman bands of the herring sperm DNA molecules. SERS spectra were collected in 10 random points of the silvered porous silicon substrate. Remarkably the silvered PS demonstrates SERS activity for all three lasers.

The following SERS mapping of the substrates allowed us to detect identifiable SERS spectra of the herring sperm DNA collected under each laser excitation (**Fig. 1-II-5A**).

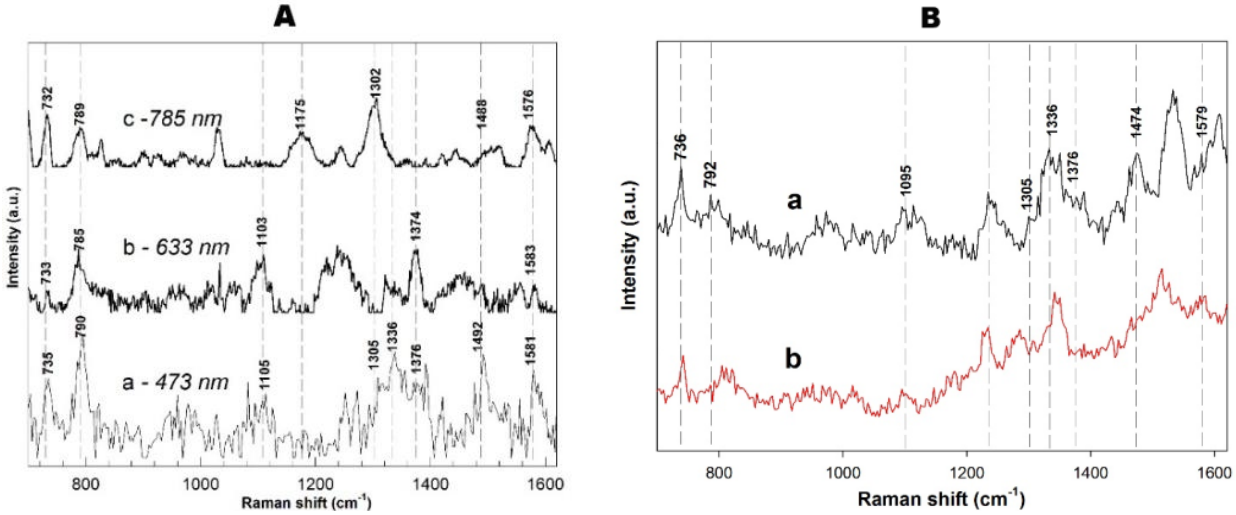

***Fig. 1-II-5.** (**A**) SERS spectra of the 10–8M herring sperm DNA adsorbed on the surface of the silvered PS collected at excitation wavelengths of 473, 633 and 785 nm. (**B**) SERS spectra of the 10–8M (a) and 10–10M (b) herring sperm DNA adsorbed on the surface of the silvered PS. The spectra were collected at an excitation wavelength of 473 nm.*

Finally, the SERS mapping was used to detect the herring sperm DNA at an extremely low concentration of 10^{-10} M. In **Fig. 1-II-5B** the comparison of two SERS spectra of the DNA

molecules at different concentrations is presented. The SERS spectra were recorded at an excitation wavelength of 473 nm since both red and near-IR lasers showed no results for the lowest concentration.

The results of these studies suggest that the classical spectra of DNA molecules can be found by the SERS substrate mapping. Moreover, the prospects for the DNA detection by the SERS spectroscopy with lasers of 473, 633, and 785 nm wavelengths are very encouraging. To our knowledge, the detection of such a small amount of DNA has not been reported previously.

2.3. Photo- and upconversion luminescence of transparent glass-ceramics based on ZnO nanocrystals activated with rare earth elements.

In 2016, new impressive results were obtained in the sphere of photo- and upconversion luminescence activities. As phosphor we employed transparent zincite (ZnO) glass-ceramics obtained from the initial glass matrices by secondary heat treatment at 680-860°C. The average crystal size obtained from the X-ray diffraction data was found to be in the range between 14 and 35 nm (**Fig. 1-II-6**).

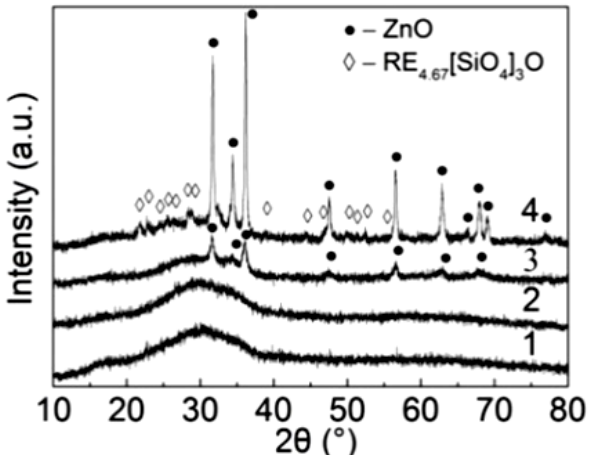

Fig. 1-II-6. *XRD patterns of the initial glass co-doped with 1 mol% Eu_2O_3 and 1.5 mol% Yb_2O_3 (1), initial glass co-doped with 1 mol% Eu_2O_3 and 1 mol% Yb_2O_3 (2) and GC doped with 1 mol% Eu_2O_3 and 1 mol% Yb_2O_3 and heat-treated at 680 ℃ for 12 h (3) and at 860 ℃ for 2 h (4).*

The luminescence properties of the glass and glass-ceramics were studied by measuring their excitation and emission spectra at 300, 78, and 4.2 K. The results are presented in **Fig. 1-II-7** (1,2,3). Strong red emission of Eu^{3+} ions dominated by the $^5D_0$–$^7F_2$ (612 nm) electric dipole transition was detected. Changes in the luminescence properties of the Eu^{3+}-related excitation and emission bands were observed after heat treatment at 680°C and 860°C. The ZnO nanocrystals showed both broad luminescence (400-850 nm) and free-exciton emission near 3.3 eV at room temperature.

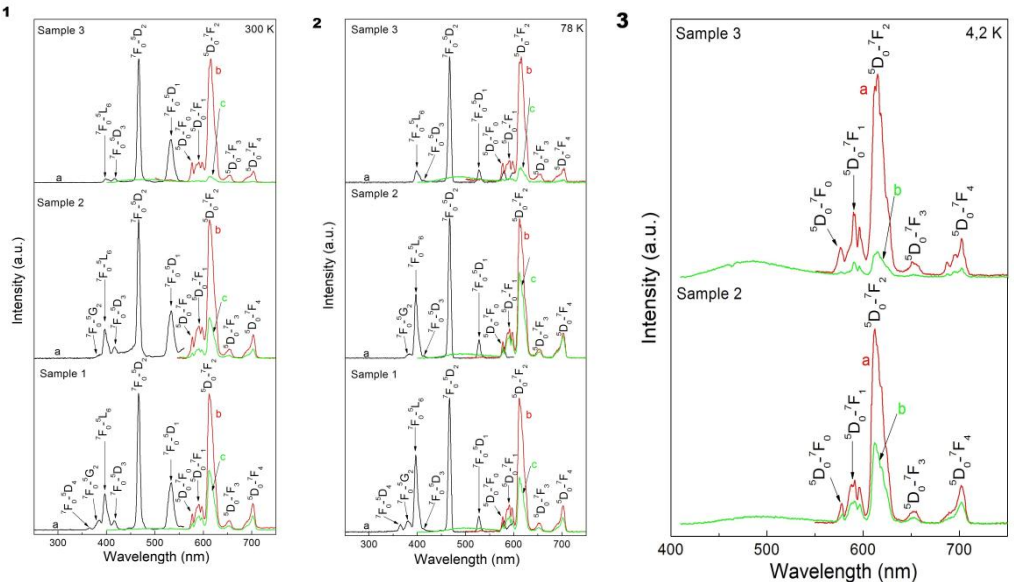

Fig. 1-II-7. (1) *Normalized luminescence excitation spectra (a) and luminescence spectra for glass and GC recorded for excitation wavelengths of λ_{ex} ~ 467 nm (b) and λ_{ex} ~ 397 nm (c) at room temperature.* ***(2)****Normalized luminescence excitation spectra (a) and luminescence spectra for glass and GC recorded for excitation wavelengths of λ_{ex} ~ 467 nm (b) and λ_{ex} ~ 397 nm (c) at liquid nitrogen temperature.* ***(3)*** *Luminescence spectra for GC recorded for excitation wavelengths of λ_{ex} ~ 467 nm (a) and λ_{ex} ~ 397 nm (b) at liquid helium temperature.*

The upconversion luminescence spectrum of the initial glass was obtained under excitation of a 976-nm laser source. A simplified energy level diagram for Eu^{3+}/Yb^{3+} ions and corresponding UCL spectrum are demonstrated in **Fig. 1-II-8 (a,b)**, respectively. The CIE color coordinates corresponding to the UCL of the sample under investigation are estimated to be (x=0.59, y=0.34). They are located in the orange-reddish region (**Fig. 1-II-8 (c)**).

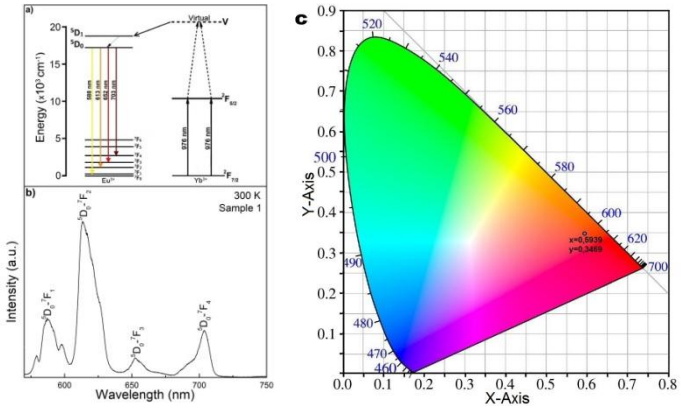

Fig. 1-II-8. *Schematic energy level diagram of Eu^{3+}/Yb^{3+} ions* ***(a)*** *and UCL spectrum of sample 1 recorded at room temperature under 976 nm laser excitation* ***(b)****, CIE diagram of Eu^{3+}, Yb^{3+} co-doped initial glass* ***(c)****.*

Thus, in transparent glass-ceramics from the potassium-zinc-aluminum-silicate system co-doped with rare-earth ions (europium, ytterbium) and containing ZnO nanocrystals, strong red (~612 nm) luminescence in the visible region from intracenter transitions on Eu^{3+} ions and ultraviolet exciton luminescence (~380 nm) from ZnO crystals have been simultaneously observed

for the first time. Luminescence from triply charged europium ions has never been studied for this type of glass-ceramics.

3.0. Guest seminar

On October 16, 2016 a head of FLNP sector of Raman spectroscopy G.M.Arzumanyan gave a guest seminar at the A.M.Prokhorov General Physics Institute of the Russian Academy of Sciences (GPI RAS) in Moscow. The aim of his report was to familiarize the participants with a multimodal optical platform at JINR allowing one to conduct investigations in the field of spontaneous and stimulated Raman scattering, as well as with the first joint unique results on coherent surface-enhanced Raman scattering. A monolayer of molecules of 3,3'-dithiobis (6-nitrobenzoic acid, DTNB) adsorbed onto the surface of a dielectric metamaterial with gold nanoparticles immobilized on a nanostructured faceted surface of cerium dioxide film was used as a model sample. The Raman shift at 1344 cm^{-1} which is characteristic of the sample was used for surface-enhanced coherent mapping of the signal intensity with high contrast and high spatial resolution. The unique technique of registration of such signals has been developed at JINR (Dubna) in close cooperation with GPI RAS, ITAE RAS, MSU and IBCP RAS.

In the final discussion it was noted that the optical platform based on the "CARS" microscope at JINR can be considered as one of the best instruments in Russia for high-contrast and high-sensitive research in the field of Raman spectroscopy and microscopy.